## Highlights:

- PCM nanoemulsions were prepared by low-energy emulsification methods.
- Brij L4 was applied as emulsifier at 5-15% mass concentrations.
- Smallest droplet size was 60 nm and remained stable over 15 months.
- Supercooling was reduced with nano $SiO_2$ as nucleating agent.

Submitted to *Solar Energy Materials and Solar Cells*

(Original Research Ms)

Revised Ms. SOLMAT-D-20-00399

# Evaluation and manipulation of the key emulsification factors toward highly stable PCM-water nano-emulsions for thermal energy storage

Xiyao Zhang [a], Jianlei Niu [b], Jian-yong Wu [a] *

[a] Department of Applied Biology & Chemical Technology, [b] Department of Building Service Engineering, The Hong Kong Polytechnic University, Hung Hom, Kowloon, Hong Kong

* Corresponding author: jian-yong.wu@polyu.edu.hk

**Abstract**

PCM emulsions represent a common type of fluid media for thermal enenergy storage (TES) systems. However, a major challenge for their application is to maintain a stable homogeneous fluid. Reduction of the droplet size is one of the most effective approaches for improving stability, such as the preparation of nano-emulsions. This work aims to develop stable PCM-water nano-emulsions prepared with n-hexadecane by manipulating the key emulsification factors, particularly the emulsifer combinations and process conditions. Two low-energy emulsification methods, phase inversion temperature (PIT) and emulsion inversion point (EIP), were applied to prepare the nano-emulsions, using Brij L4 as the emulsifier. Several important properties of the emulsions were evaluated including droplet size distribution, conductivity, and rheological characteristics and the stability of emulsions over extended periods and multiple freeze-thaw cycles. Moreover, the thermal performance for their potential application in TES systems were examined. Eventually, nano-emulsions with small and uniform droplets were obtained by both PIT and EIP methods with suitable emulsifier concentrations. The smallest droplet size (~60 nm) was attained with 11% emulsifier and 30% PCM by the PIT method, and the most stable emulsion attained with 15% of emulsifier and 30% of PCM. The PCM nano-emulsions behaved as a Newtonian liquid with a good fluidity and a superior stability over long-time storage and freezing-cycles. The degree of supercooling was reduced with the addtion of nano $SiO_2$ as a nucleating agent. The findings from the study are useful for better understanding of the controlling factors and further development of stable and effective nano-emulsions.

**Keywords:** Phase change material; n-Hexadecane; Nano-emulsion; Stability; $SiO_2$ nucleating agent; Supercooling

## 1. Introduction

Thermal energy storage (TES) is widely recognized as one of the most promising means for integration of renewable energy into the power supply and the demand sides in flexible scales [1, 2]. By storage of thermal energy at the desired temperature ranges, TES is effective to increase the efficiency of electric power, facilitate large-scale switching and utilize natural energy resources such as solar and geothermal heat. Among various TES systems, the latent heat storage using phase change materials (PCMs) is most favorable because of its compact

size and nearly constant operating temperature [3]. PCMs are capable of releasing and absorbing a large amount of thermal energy during their phase change processes.

PCM emulsions represent a major type of storage media for TES with the advantages of a high energy storage density in a narrow temperature range and rapid charging rates from the enlarged interface area [4, 5]. However, a major challenge for its application is to maintain a stable homogeneous fluid [6]. Reduction of the droplet size is one of the most effective approaches for overcoming instability. Nano-emulsions of PCMs with small droplets of 20-500 nm dispersed in water with the aid of emulsifiers can retain a high stability and long service life [7]. PCM nano-emulsions are also much less sensitive to dilution and variation of temperature and pH than micro-emulsions and regarded as the promising energy storage media for TES systems [8]. In addition, the phase inversion preparation of a nano-emulsion is nearly spontaneous by changing the surrounding temperature and/or mass fraction of components, favoring industrial scale-up.

The formation of emulsions can usually be achieved by high-energy or low-energy methods [9]. High-energy emulsification strategies require the use of high energy for mechanical stirring, high-pressure homogenizers, or ultrasound generators to prepare tiny droplets. In contrast, low-energy emulsification methods utilize the chemical energy stored in the ingredients to produce emulsions nearly spontaneously, offering a greater potential for industrial applications. A common low-energy method is by changing the temperature of system to affect the transition from an O/W emulsion at a low temperature to a W/O emulsion at a high temperature (transitional phase inversion), and vice versa. During the heating or cooling process, the system passes through an extremely low interfacial tension region achieved at the hydrophilic-lipophilic balance (HLB) temperature or the phase inversion temperature (PIT). The PIT method is based on this phenomenon to facilitate the formation of well-dispersed oil droplets [10-12].

Phase inversion can also be accomplished by altering the volume fraction of water, called the emulsion inversion point (EIP) method [12]. By gradual addition of water into oil, water droplets are formed in a continuous oil phase initially. As the volume fraction of water increases to a point so that the emulsion is converted from a W/O to an O/W, which is the inversion point.

During this transition, the minimal interfacial tension is achieved to promote the formation of fine droplets [12-14]. Liu et al. [15] prepared paraffin-in-water nano-emulsions by the EIP method and attained a nano-emulsion with a minimum droplet radius of 74 nm at an optimum HLB value and temperature. Xin et al. [16] prepared the paraffin nano-emulsion with Tween 20 and Span 20 by EIP method. They found that the addition of both ionic surfactants sodium dodecyl sulfate (SDS) and cetyltrimethylammonium bromide (CTAB) decreased the mean droplet size (<150 nm). The stability of the nano-emulsion was enhanced with SDS but decreased with CTAB, due to different electrostatic interactions between droplets.

Schalbart et al. [17] prepared a tetradecane nano-emulsion as a refrigerant by the PIT method, with a narrow droplet size distribution of 200-250 nm. This emulsion remained stable without sedimentation and creaming for more than 6 months and a low viscosity only about 2-4 times that of water. However, Ostwald ripening destabilization occurred, resulting in an increase in the droplet size and a decrease in viscosity. Schalbart and Kawaji [18] investigated the thermal properties and stability of a series of paraffin nano-emulsions with average droplet sizes of 150-250 nm. The emulsions were stable for 30 freezing and melting cycles over a period of one week, and the supercooling degrees and other thermal properties were similar to those of n-hexadecane/water micro-emulsions (droplet sizes >1 μm) by our group [19].

Jadhav et al. [20] prepared a paraffin nano-emulsion with SDS as the emulsifier under the effect of ultrasound. The mean droplet diameter of the emulsion with the optimal formula and process was 160 nm, and the emulsion was more stable than that prepared with the same formula by the EIP method. Kawanami et al. [21] produced PCM nano-emulsions by the D-phase method with hexadecane and tetradecane as the PCMs but observed a large supercooling degree of 17 °C. Chen and Zhang [22] also prepared PCM nano-emulsions by the D-phase method with n-hexadecane and n-octadecane as PCMs, which had average droplet sizes of 290 nm and 320 nm, respectively. Zhang and Zhao [23] synthesized a novel PCM nano-emulsion with the minimum diameter of 117 nm by the direct mini-emulsion method. It was found that the mass fraction of PCM had a great impact on the particle size distribution of nano-emulsions. Large supercooling and Newtonian fluid behavior were observed in these studies. Cabaleiro et al. [24]

used a commercial paraffin wax to prepare PCM nano-emulsions with droplet sizes of ~90-150 nm through the solvent-assisted method. Although a highly stable nano-emulsion was attained, the supercooling effect persisted (up to 3.2 K) even with multiple approaches.

Supercooling refers to the phenomenon that a liquid starting to freeze at a temperature below its melting temperature. Previous studies have mostly directed at emulsification and stability mechanisms of nano-emulsions, but made little effort to addressed the supercooling. Supercooling increases the operation temperature range of TES systems, leading to a lower energy storage efficiency [25]. The addition of impurities as nucleating agents catalyzing nucleation, such as homologous compounds with higher melting temperatures [26], suitable surfactants [27] and solid particles [19, 28-30], is regarded as an effective approach to reducing the degree of supercooling in PCM emulsions with micro-sized droplets. However, this approach is questionable for PCM nano-emulsions because it is very hard to disperse the nucleating agents effectively into the small nanosized droplets. By and large, it is of significance to conduct further and more systematic assessment of the nano-emulsions aiming for TES applications.

This study was to evaluate comprehensively the emulsifier materials and process conditions for preparation of stable n-hexadecane nano-emulsions in water. Various formulae and factors on nano-emulsion properties were taken into consideration including the emulsifier concentration, dispersed phase contents, salt and nanoparticle additives. The stability of emulsions was evaluated over extended period of time and for multiple freezing-thawing cycles. The physical principles and theoretical basis were further elaborated to gain better understanding of the factors and effects on stability. The performance indicators for their potential application in TES systems were also examined, including conductivity, thermal performance, degree of supercooling and rheology characteristics.

## 2. Materials and methods

### 2.1. Materials

As in our previous study [7], n-hexadecane $C_{16}H_{34}$ (99%) was used as the PCM (International Laboratory, USA) and non-ionic surfactant Brij L4 as the emulsifier (analytical grade, Sigma-

Aldrich). Hydrophobic $SiO_2$ nanoparticles (NPs) in the range of 7- 40 nm were used as the nucleating agent according to the previous study [7] (Hydrophobic-230, 99.8% metal basis, Aladdin, China).

### 2.2. Preparation of PCM nano-emulsions

The PCM nano-emulsions were prepared by two low-energy phase inversion emulsification methods in six sets of conditions as shown in Table 1. With the PIT method, demineralized water was slowly added at about 5.0 mL $min^{-1}$ to a mixture of n-hexadecane and emulsifiers on a magnetic stirrer at 400–600 rpm and 60 °C (the temperature was set according to the phase inversion temperatures of samples), and then cooled down to room temperature (20 °C). With the EIP method, demineralized water was added at about 1.0 mL $min^{-1}$ to a mixture of n-hexadecane and emulsifiers on a magnetic stirrer at 400–600 rpm and room temperature (20 °C).

Table 1 Experimental variables and conditions for preparation of PCM-water nano-emulsions

| Variable | Total emulsifier | Oil-surfactant ratio | PCM content | Method |
|---|---|---|---|---|
| 1. Emulsifier concentration | 5-15% | By samples | 30% | EIP/PIT [a] |
| 2. O/W ratio 1:1-3 | By samples | 2 | By samples | EIP/PIT |
| 3. PCM content | 15% | By samples | 10-50% | EIP/PIT |
| 4. Salt concentration 0-2 % | 13% | 2.3 | 30% | EIP |
| 5. NP concentration 0-4 % | 13% | 2.3 | 30% | EIP |

a. PIT: phase inversion temperature; EIP: emulsion inversion point.

### 2.3. Characterization of emulsion droplets

The size distribution of emulsion droplets was determined by DLS with the use of a laser diffraction particle size analyzer (Malven Zetasizer: Model Nano ZS), which had a broad measuring range of 0.02 μm to 5,000 μm. A total of 100 measurements were performed for 20 min at a scattering angle of 90° at 25 °C. The average particle size (in nm) and the polydispersity index were analyzed using the Zetasizer Software. Conductivity was measured to identify the type of emulsion (W/O or O/W), using a digital conductivity meter with a Pt/platinized electrode (Traceable, China).

### 2.4. Thermal analysis

A differential scanning calorimeter (Mettler Toledo DSC 3) with aluminum crucibles was used to determine the melting and nucleation temperatures, and the thermal data were analyzed and plotted using the STARe software. Temperature and sensitivity were calibrated using standard materials at heating/cooling rate of 5 °C/min. The samples were initially kept at −5 °C for 10 min to facilitate stabilization, then heated to and maintained at 30 °C for 10 min, and finally cooled to −5 °C.

The onset temperature for melting/crystallization can be observed as a deviation from the baseline, and is independent of the heating/cooling rate [31]. The temperature difference between melting and crystallization is the supercooling degree. When multiple peaks existed, the main peak was used for calculating the supercooling degree.

### 2.5. Rheometry

The apparent viscosity of emulsion samples was determined using a rotational viscometer with an ultra-low viscosity adapter (Brookfleld, DV3T). The measurement range was from 6.4 to $2\times10^7$ mPa·s and the accuracy was 1%. For emulsions with non-Newtonian behavior, the apparent viscosities at a low shear rate (0.6 $s^{-1}$) were compared for evaluation of the emulsion viscosity performance.

### 2.6. Evaluation of the stability of the PCM–water emulsion

The storage stability of the emulsions was evaluated by visual observation of the droplet size and phase separation after the storage period and repeated thermal cycles. The standard procedure for testing the stability of the PCM emulsions under thermal cycles is to subject them to multiple freezing–thawing cycles [32]. In this study, each cycle included two steps, freezing in an ice-water bath for 30 min and then melting in air to room temperature (25 °C) for 30 min.

## 3. Results and discussion

### 3.1. Effects of emulsifier concentration

Fig. 1 shows the appearance (with photos Fig. 1a) and various characteristics of PCM-water

emulsions prepared with various concentrations of Brij L4 by EIP and PIT methods (Fig. 1b-e). At a concentration below 7% with the PIT method and below 11% with the EIP method, Brij L4 failed to disperse the PCM emulsion into uniform nano-droplets. The smallest average droplet sizes were 59.8 nm with 11% of emulsifier by PIT method and 126.5 nm with 13 % of emulsifier by EIP method, respectively, while a higher concentration of Brij L4 resulted in larger droplets due to the higher viscosity. The average droplet sizes of emulsions by the EIP method were larger than those by the PIT, owing to the energy input and the phase inversion processes at different temperatures and viscosities (Fig. 1b; Fig. 1c). The higher temperature with the PIT method provides more energy into the system, increasing the interface free energy and also lowers the viscosity, reducing to the droplet size. On the other hand, the longer period of time in the EIP process allows the instability of droplet to develop, especially at a low viscosity. When the emulsifier concentration was relatively high (11-15 %), fine nano-emulsions could be produced by both methods, as shown by the clear nano-emulsion samples in Fig 1a.

Most of the emulsion samples behaved as Newtonian fluids at the room temperature, which had a relatively stable apparent viscosity and varied slightly with the shear rate Fig. 1d. The samples with 5 % of emulsifier behaved as non-Newtonian fluids due to their polydisperse distributions, allowing them more likely to perform as normal emulsions. The apparent viscosity increased with emulsifier concentration and the sample with 15 % of emulsifier had
the highest apparent viscosity of 168.4 mPa.s at 0.6 $s^{-1}$, while all other samples had an apparent viscosity below 50 mPa.s. As shown in Fig. 1e, the emulsion conductivity was relatively high in the lower temperature range but dropped sharply at a higher temperature point, indicating the phase inversion temperature (PIT) from O/W to W/O. The PIT point decreased with the emulsifier concentration, but at much higher concentrations, the conductivity plots showed a second maximum due to the presence of a bi-continuous phase [33].

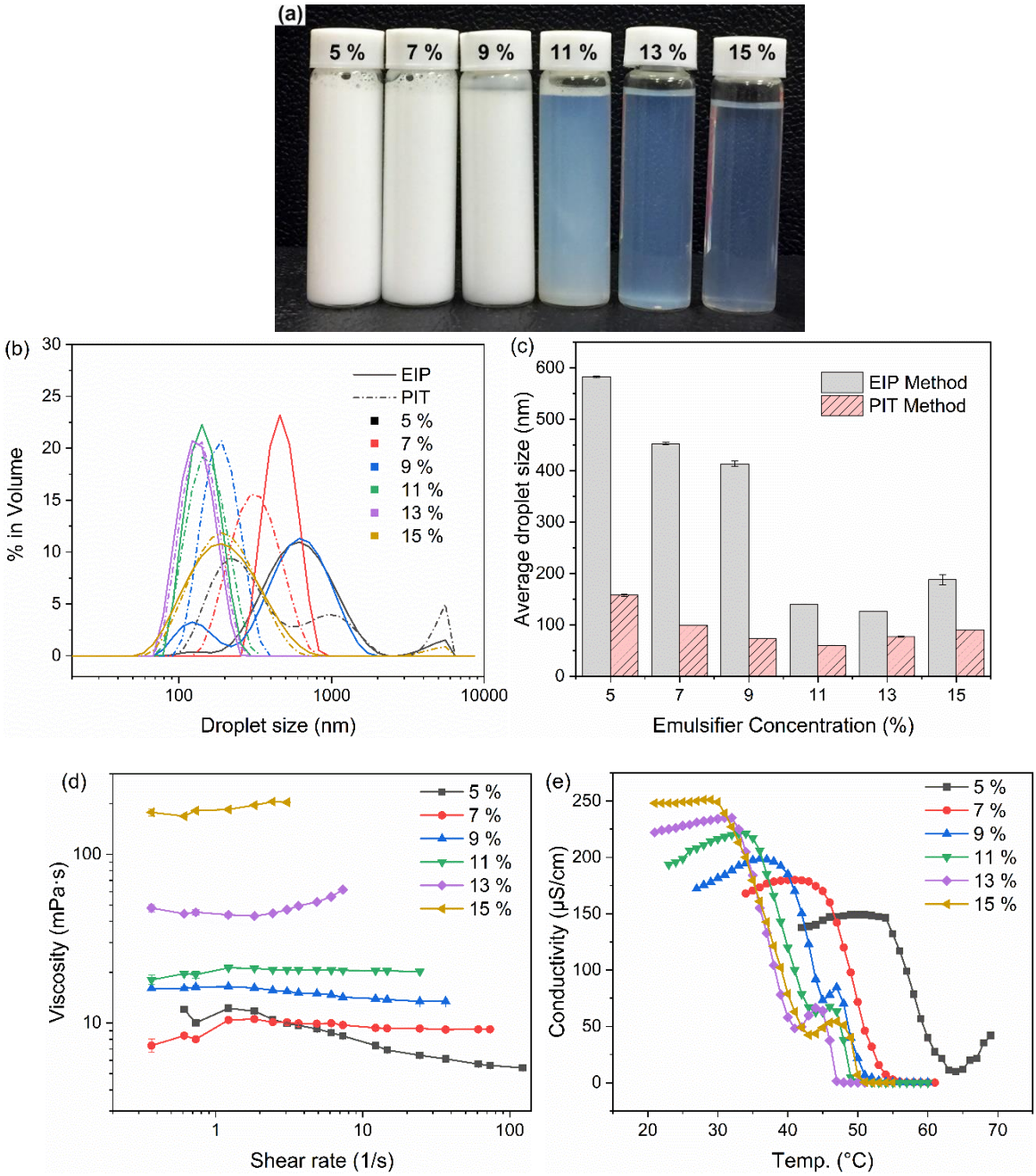


**Fig. 1** (a) The appearance of nano-emulsion samples with Brij L4 at 5-15 wt % by the EIP method; (b) Droplet size distribution and (c) Average droplet size for the nano-emulsion samples prepared using different Brij L4 concentration and methods, with a PCM mass fraction 30 % and an emulsifier total concentration 5-15%; (d) Variation in apparent viscosity with the shear rate; and (e) conductivities with the temperatures for the nano-emulsion samples with various concentrations of Brij L4, with 30 % PCM by PIT method.

### 3.2. Effects of the oil-water ratio

As seen from the photos of the emulsion samples prepared with different oil/water ratios and a constant oil-surfactant ratio of 2:1 (Fig. 2a), clear nano-emulsions were obtained at all three O/W ratios. The droplet size distributions of the samples were similar, and their average sizes were not much dependent on the amount of water, suggesting that the oil-surfactant ratio be the determining factor for the droplet size. Nevertheless, the droplet size distribution still varied slightly with the O/W ratio and the preparation method, PIT or EIP (Fig. 2b). The average droplet sizes of samples by EIP method were larger than those by PIT at the O/W ratio of 1:3 and 1:2 (Figure 2 c), similar to the results in the former section. However, the average droplet size of the sample by the EIP method was smaller than that by PIT at the O/W ratio of 1:1, which was attributed to the higher viscosity in the PIT process. The emulsifier consists of amphiphilic molecules which absorb on interface area between phases. When the emulsifier concentration reaches the critical micelle concentration (CMC), its molecules start to aggregate into super-molecular structures such as micelles, leading to a dramatic increase in viscosity [34]. Hydrophobic interactions are the driving forces for the aggregation as the polar head groups of emulsifier molecules are hydrated to allow appreciable water–amphiphile contact in the micelles. At relatively high concentrations, the emulsifier self-aggregation leads to such structures as lamellar, liquid crystalline, sponge-like, vesicular, and bi-continuous microemulsion phases [35]. CMC is sensitive to temperature and the CMC of non-ionic emulsifiers decreases with temperature, and to the lowest at 50 °C [36]. Therefore, the emulsion prepared at O/W ratio 1:1 in the PIT process had a significantly higher viscosity (Fig. 2d). As shown in Fig. 2e, the plot of emulsion conductivity versus temperature for the nano-emulsion samples, the PIT points were 29 °C, 24 °C and 28 °C, respectively, but did not show an obvious trend with the O/W ratio.

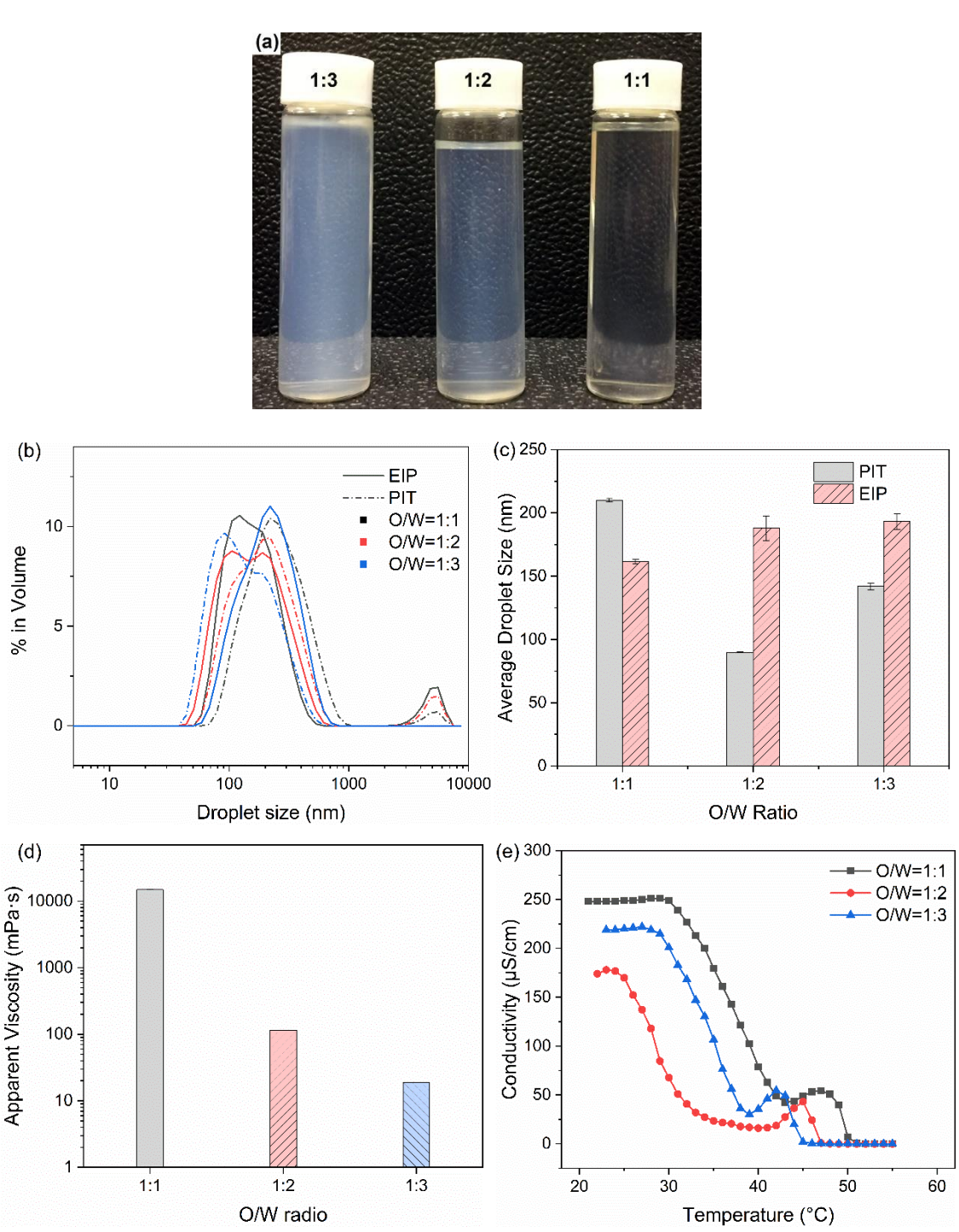


**Fig. 2** (a) The appearance of nano-emulsion samples by the EIP method; (b) Droplet size distribution; (c) average droplet sizes; (d) apparent viscosities at the shear rate of 0.6 $s^{-1}$; and (e) variations in conductivities with the temperatures for the nano-emulsion samples prepared with various O/W ratios and using different methods, with the constant oil-surfactant ratio at 2:1. Error bars represent standard deviations (SD), $n$ = 3.

### 3.3. Effects of the PCM mass fraction

Fig. 3 shows the characteristics of PCM nano-emulsions with different mass fractions of PCM at a fixed emulsifier concentration of 15%. By direct observation (Fig. 3a), with the increase in PCM mass fraction, the emulsion turned from milky to a clear liquid at 30%, but changed to cloudy again with a further increase in PCM content. Fig. 3b shows the droplet size distribution of the emulsion samples and Fig. 3c their average droplet sizes. Nano-emulsions could be prepared with the PCM mass fraction in the range from 20% to 50%. When the PCM mass fraction was lower, it was difficult to form a uniform water-in-oil emulsion during the PIT process and the excess emulsifier increases the viscosity and emulsifier micelles hinders the phase inversion process (Fig. 3d). The smallest droplet size was attained with 40% of PCM, 60.63 ±1.21 nm by PIT and 61.65 ± 0.70 nm by EIP, though the viscosity was high due to the high dispersed phase fraction as shown in Fig. 3c.

There was also a reverse trend in their viscosity (Fig. 3d). Very high apparent viscosity values were observed with low or high mass fractions of PCM but a much lower viscosity with 30% of PCM. (The viscosity of the sample with 50% of PCM was out of the measurement range of viscometer). In general, when the dispersed fraction is low, an excess of emulsifier forms micelle structures which limits the molecular movements, resulting in a high viscosity. Besides, increasing the mass fraction of the dispersed phase can also increase the viscosity due to increasing interactions among droplets (will be further explained in section 3.7 later). Each of the above mechanisms can contribute to a higher viscosity of an emulsion. In practice, one of the mechanisms usually dominates, depending on the composition of the product and its effect on viscosity. In this case, at a low dispersed phase content (< 30 wt% ), the effect of emulsifier dominates but at high disperse phase content, those due to concentrated droplets of the emulsion dominate. As shown by the plots of conductivity versus temperature (Fig. 3e), the PIT point changed in a way nearly opposite to the viscosity and reached its maximum at 30% of PCM.

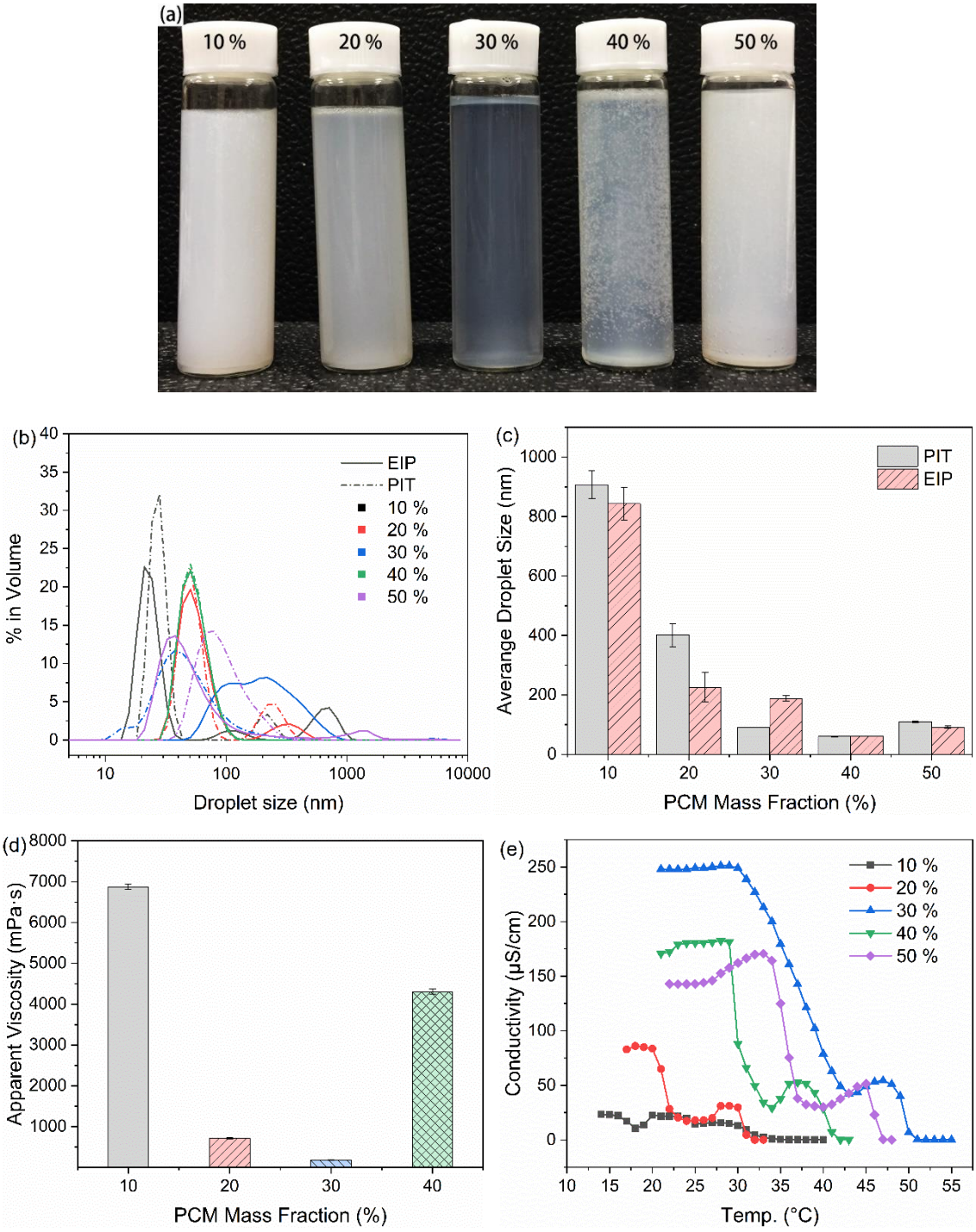


**Fig. 3** (a) The appearance of nano-emulsion samples by the EIP method; (b) Droplet size distribution; (c) Average droplet size; (d) Apparent viscosity; and (e) Variations in conductivities with the temperatures for the nano-emulsion samples prepared using different mass fraction of PCM by methods, with 15% emulsifier and 10-50% PCM content.

### 3.4. Effects of NaCl salt

The addition of an ionic agent such as NaCl to the emulsions can reduce the electrostatic repulsion and facilitate the aggregation of droplets due to attractive interactions, but can remain stable and avoid coalescence [37]. Moreover, while the droplets deform slightly, they tend to form a random network instead of a compact floc. PCM nano-emulsions with different concentrations of NaCl were prepared by the EIP method at 30% PCM and 13% emulsifier. The appearance of the sample was translucent and gradually became cloudier as the NaCl concentration increased (Fig. 4 a). The nano-emulsion with NaCl had a smaller droplet size compared with the sample without ions (Fig. 4 b).

As shown in Fig. 4c, the apparent viscosity showed a moderate increase with 0.5-1% of NaCl but dramatically with 2% of NaCl added to the nano-emulsions. In addition, the nano-emulsions all showed a shear-thinning behaviour at all salt concentrations. As shown in Fig. 4d, the conductivity of emulsion samples was higher at a lower temperature and decreased sharply at a higher temperature point, indicating the phase inversion from O/W to W/O. In the relatively low temperature range, the conductivity was much lower with the addition of NaCl, due mostly to the formation of net structures, restricting the motion of ions. The conductivity showed a sharp increase at the PIT point, which was corresponding to the transition to bi-continuous phase [33]. The PIT point had no obvious change with the salt except for a slight increase in the sample with 2% NaCl, due probably to its high viscosity.

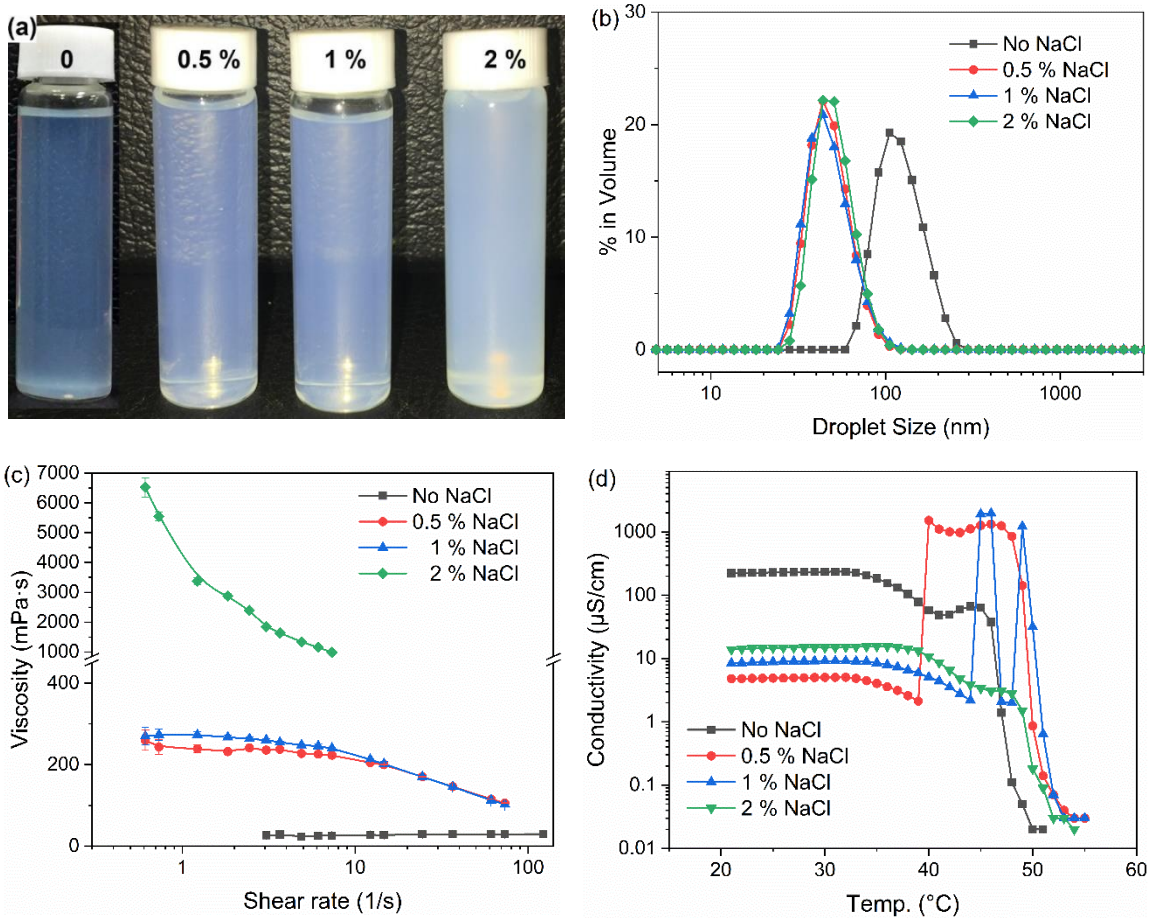


**Fig. 4** (a) The appearance, (b) Droplet size distribution, (c) Variation of apparent viscosity with the shear rate and (d) Variation of conductivities with temperatures for the nano-emulsion samples prepared with different concentrations of NaCl by the EIP method, with the constant PCM and surfactant concentration at 30% and 13%, respectively. Error bars for SD, $n$ = 3.

### 3.5. Effects of solid NPs

The hydrophobic $SiO_2$ NP, which was used as an effective nucleating agent in our previous studies [7, 28], was applied to the nano-emulsions. The NPs were dispersed in the PCM liquid by sonication in an ultrasonic bath for 1 hour before emulsification. PCM nano-emulsions with different concentrations of $SiO_2$ NPs were then prepared by the EIP method, with a PCM mass fraction of 30% and a surfactant concentration at 13%. The emulsion was translucent and slightly cloudier than without NPs (Figure 5 a). As shown in Figure 5 (b), the nano-emulsion with the NPs had a similar droplet size distribution and smaller average droplet size compared with the sample without NPs.

On the other hand, the addition of NPs increased the viscosity of nano-emulsions (Fig. 5c). The apparent viscosity of emulsion was slightly increased with 0.5-1.5% but quite notably with 2% and 4% of $SiO_2$ NPs. In addition, the PCM nano-emulsion behaved as a Newtonian liquid at relatively low NP concentration range but turned to a shear thinning liquid at 2-4%. Interestingly, the samples with 4% of NPs had a lower apparent viscosity than that with 2% NPs, which was due probably to a smaller number of droplets with a larger droplet size. Despite the results from DLS, the change in the transparency of emulsions samples with the NP concentration indicates the increase in droplet size.

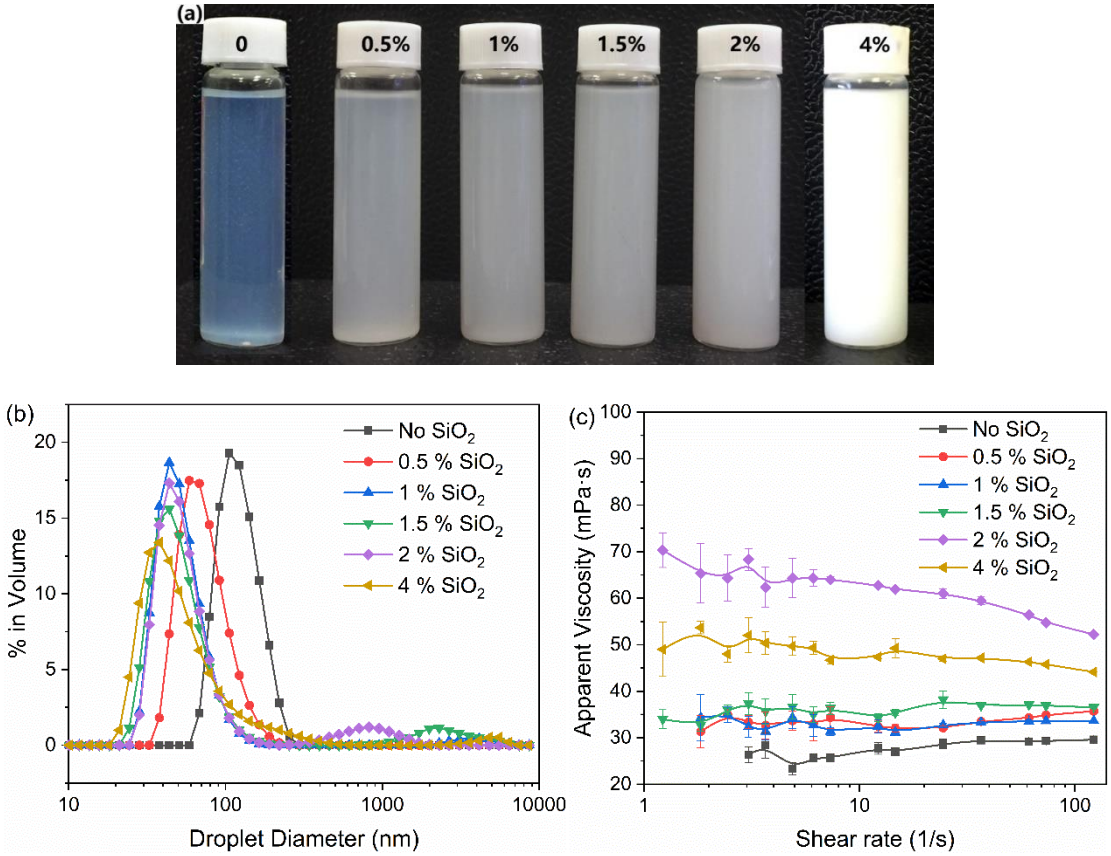


**Fig. 5** (a) The appearance, (b) Droplet size distribution and (c) Variations in apparent viscosity with the shear rate of the nano-emulsion samples with different concentrations of $SiO_2$ NPs, with a PCM mass fraction of 30%, a surfactant concentration at 13% and produced by the EIP method. Error bars for SD, $n = 3$.

Fig. 6 shows the DSC curves and the effects of NPs on supercooling, from which the melting and crystallization properties were estimated and shown in Table 2. Without the nucleating agent, the bulk PCM had a low degree of supercooling, while the nano emulsion showed a high

supercooling degree of 8.93°C due to the more restricted random homogeneous nucleation with decreasing volume [19]. The melting temperature of the nano-emulsion was also decreased with the emulsifier [38]. However, the NP nucleating agent was not as effective as in the ordinary PCM emulsions, giving rise to multiple peaks in the freezing curves of nano-emulsion samples. The nucleating agent was partially effective to reduce supercooling, which is a similar phenomenon to that reported by some other researchers [24]. These peaks indicate that the amount of nucleating agent was insufficient to disperse all of the nano-sized droplets, which was mostly attributed to the similar size scale of the nucleating agent to the nano-emulsion. The nucleating agent could not be easily added into a volume of tiny droplets. When the concentration of NPs reached 2% in PCM, most of the PCM droplets were crystallized near 10 °C. However, a much higher concentration of NPs at 4% added to the PCM did not further decrease the supercooling. Furthermore, addition of nucleating agent also reduced the emulsifier effect on the melting temperature and much more PCM melted near 16 °C with increasing NA.

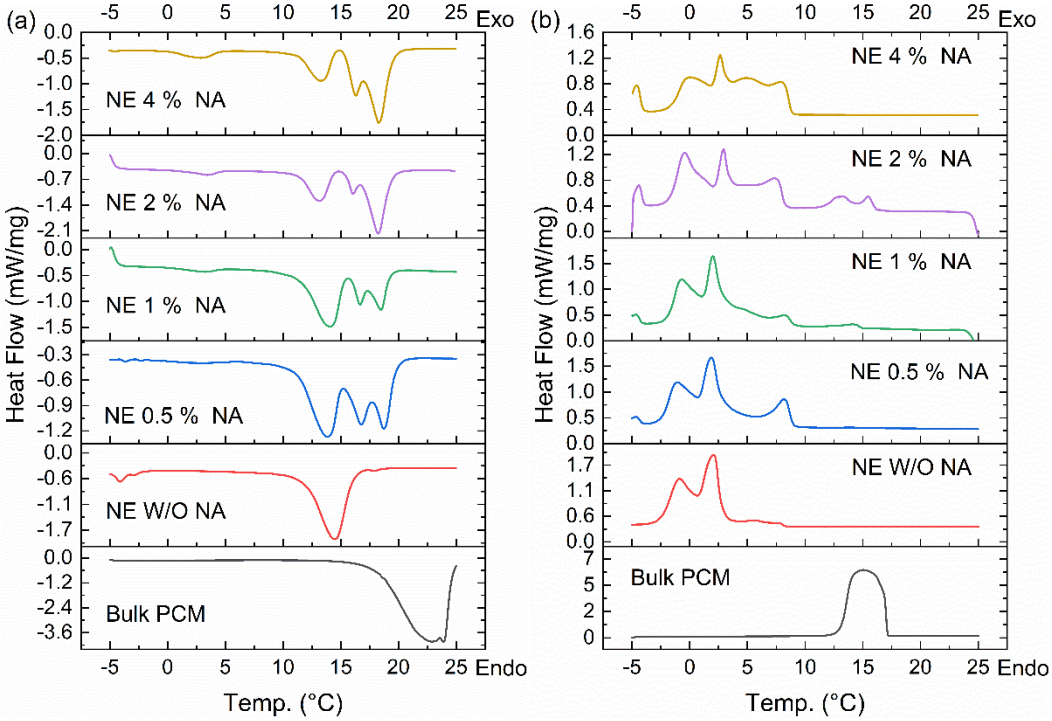


**Fig. 6** DSC curves of the PCM (nano) emulsions with various concentrations of nano $SiO_2$ NPs. The emulsion samples were with a PCM mass fraction of 30 %, and emulsifier concentrations of 13%. (a) melting curves; (b) freezing curve.

**Table 2.** Melting and freezing points of nano-emulsion (NE) samples with nucleating agent (NA).

| Samples | $\Delta H_m$ (kJ/kg) | $\Delta H_f$ (kJ/kg) | $T_{m.onset}$ (°C) | $T_{f.onset}$ (°C) | $\Delta T$ (°C) |
|---|---|---|---|---|---|
| Bulk PCM | 227.13 | 225.81 | 16.99 | 15.42 | 1.57 |
| NE 0 NA | -48.67 | 50.92 | 11.82 | 2.89 | 8.93 |
| NE 0.5% NA | -62.94 | 67.26 | 10.91/15.42 | 9.00/3.34 | 7.57 |
| NE 1% NA | -57.04 | 59.71 | 11.32/15.69 | 8.64/3.37 | 7.95 |
| NE 2% NA | -64.79 | 59.60 | 10.56/16.57 | 16.23/8.39 | 8.18 |
| NE 4% NA | -57.75 | 69.35 | 10.68/16.33 | 8.92/3.35 | 12.98 |

*Note*: $\Delta H_m$ and $\Delta H_f$ = the total transition enthalpies, and $T_{m.\ onset}$ and $T_{f.onset}$ = the onset temperatures of the melting and crystallization process, respectively. Onset temperatures of main peaks are listed with the maximum peaks underlined; $\Delta T$ = the difference of the onset temperature of the main melting peak and the freezing peak representing the degree of supercooling.

### 3.6. Stability of PCM nano-emulsions

Nano-emulsions are in a state of thermodynamic instability through the same mechanisms as for normal emulsions such as creaming or sedimentation caused by gravity, flocculation by Van der Waals attraction, Ostwald ripening by the difference in solubility between small and large droplets, coalescence by fusion between the droplets, and phase inversion between the dispersed phase and the medium interchange [39]. However, their small size results in rapid Brownian motion and a high Laplace pressure ($\Delta P=2\gamma/r$, $\gamma$ = surface tension and r = curvature radius [13]), contributing to a high resistance to deformation which is responsible for their kinetic stability to the creaming (sedimentation), flocculation and coalescence. The steric stabilization is stronger in nano-emulsions as the thickness of the adsorbed emulsifier layer (~10 nm) is comparable to the droplet size which stabilizes the emulsions against flocculation and coalescence more effectively [40].

While the nano-emulsions can become instable through various mechanisms, the initial growth of droplets generally occurs through Ostwald ripening. However, flocculation, coalescence and

creaming become more important as the droplet size increases. Therefore, Ostwald ripening is generally regarded as the dominant destabilization mechanism for nano-emulsions [8, 40, 41]. Ostwald ripening is the process mainly for the growth of large droplets at the expense of small ones in a polydispersed emulsion because of the mass transport of dispersed phase from one droplet to another through the continuous phase [42]. The mean droplet size grows according to the Lifshitz-Slyozov-Wagner (LSW) theory,

$$\frac{\mathrm{d}r^3}{dt} = \frac{8\gamma V_m C_\infty D}{9RT} \qquad (1)$$

where $C_\infty$ is the solubility of the dispersed phase in the continuous phase for a particle with infinite curvature (a planar interface), S(r) the solubility of the solute when contained within a spherical particle of radius r, $D = k_BT/6\pi\eta r$ the diffusion coefficient of the solute molecules through the continuous phase separating the droplets, $V_m$ the molar volume of the dispersed phase, $\gamma$ the interfacial tension, D the diffusivity of the dispersed phase in the continuous phase. According to this equation, the initial growth rate of the cube of the mean particle size is close to a constant but increases with an increase in the solubility of the dispersed phase and the decreases in the viscosity of the continuous phase and the droplet size.

Fig. 7 shows the emulsions recorded from one day to 15 months after preparation. The sample with 11 % emulsifier changed from a translucent to milky within 1 day, suggesting the rapid increase in the droplet size. Fig. 8a shows the changes of the droplet size of samples with time. Except for the sample with 15% of emulsifier retaining translucent over the 15 month storage period, all the remaining samples with lower concentrations of emulsifier showed a creaming layer on the top, which was due to the gravitational movement of oil droplets with a low density. This change appeared in about 7 days after the preparation of emulsion and tended to stabilize after 2 months.

As shown in Fig. 7, creaming first appeared in the nano-emulsion samples with 9-13% of the emulsifier in one week after its preparation. All samples with 5-13% of emulsifier developed a clear layer after 30 days, with the process progressing more slowly in the subsequent days, except for the one with 15% of emulsifier. According to the Stokes formula, the creaming

velocity of a dispersed droplet ($V_s=2\rho\Delta gr^2/9\eta$, :$\rho\Delta$ the difference in the densities of the dispersed and continuous phases, g: the acceleration caused by gravity, r: the droplet radius, and $\eta$: the viscosity of the continuous phase), indicating that the creaming velocity of the

droplets increased as the droplet size increased and the viscosity decreased [42]. The intense Brownian motion of droplets in nano-emulsions usually prevents the creaming process. However, the creaming phenomenon is expected to occur with the increase in droplet size by coalescence and/or Ostwald ripening. The thickness of creaming layers decreased with the concentration of the emulsifier increased, due to fewer sufficiently large droplets in the samples with higher concentrations of emulsifier.

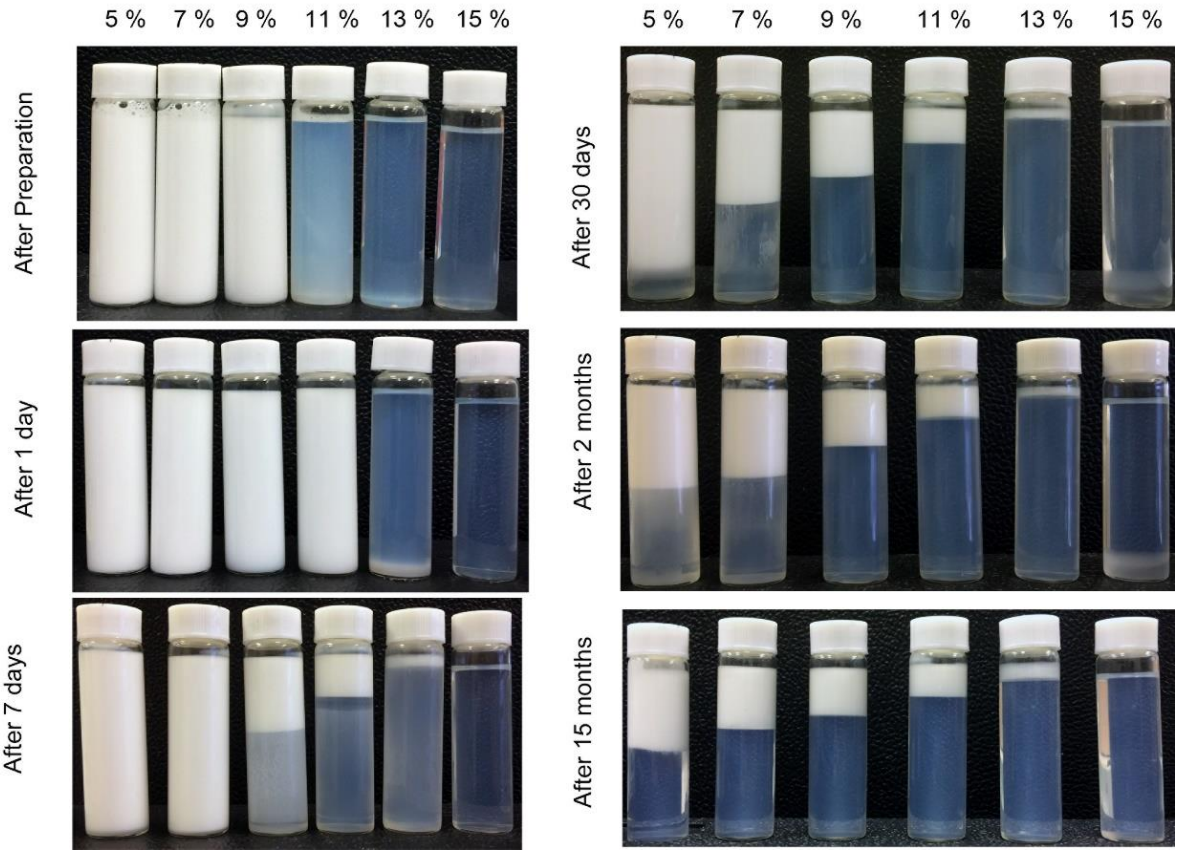


**Fig. 7** Photographs of the emulsion samples during the storage period. (Nano-emulsion samples with different concentrations of emulsifier were stored in stoppered 10 mL cylindrical bottles at room temperature).

Figs. 8a-b show the changes of the average droplet size of emulsions with different concentrations of emulsifier over a long storage period. With 5-11% emulsifier, the average droplet size grew gradually in the first 24 h and fluctuated in following period to μm scale after 15 months. However, there was no obvious change in the droplet size with 13-15% emulsifier during the whole storage period. As shown in Fig. 8c, the cubic values of average droplet sizes of samples with 5-11% emulsifier increased linearly and the linear region increases with the emulsifier concentration. This together with the slow destabilization of samples indicates that

Ostwald ripening alone governed the initial destabilization. The sample with 15% emulsifier remained stable in appearance and droplet size over the whole storage period, which could be attributed to its relatively high viscosity.

Fig. 8d shows the droplet size of all samples after thermal treatments and Figure 9 shows the corresponding photos. After 5 freeze-thaw cycles, the average diameters of the samples with 5-11% increased but the magnitude of the growth of average droplet sizes decreases with the emulsifier concentration. There was no change in the droplet size of samples with 13-15% of the emulsifier and no change in all samples after 10 cycles. All samples could re-emulsified by the PIT method, heating to 60 °C and cooling in ice-water bath, and their average droplet sizes were recovered. There was no variation in the appearance of samples nor any phase separation during the test, except for the creaming phenomenon in the sample with 11% emulsifier.

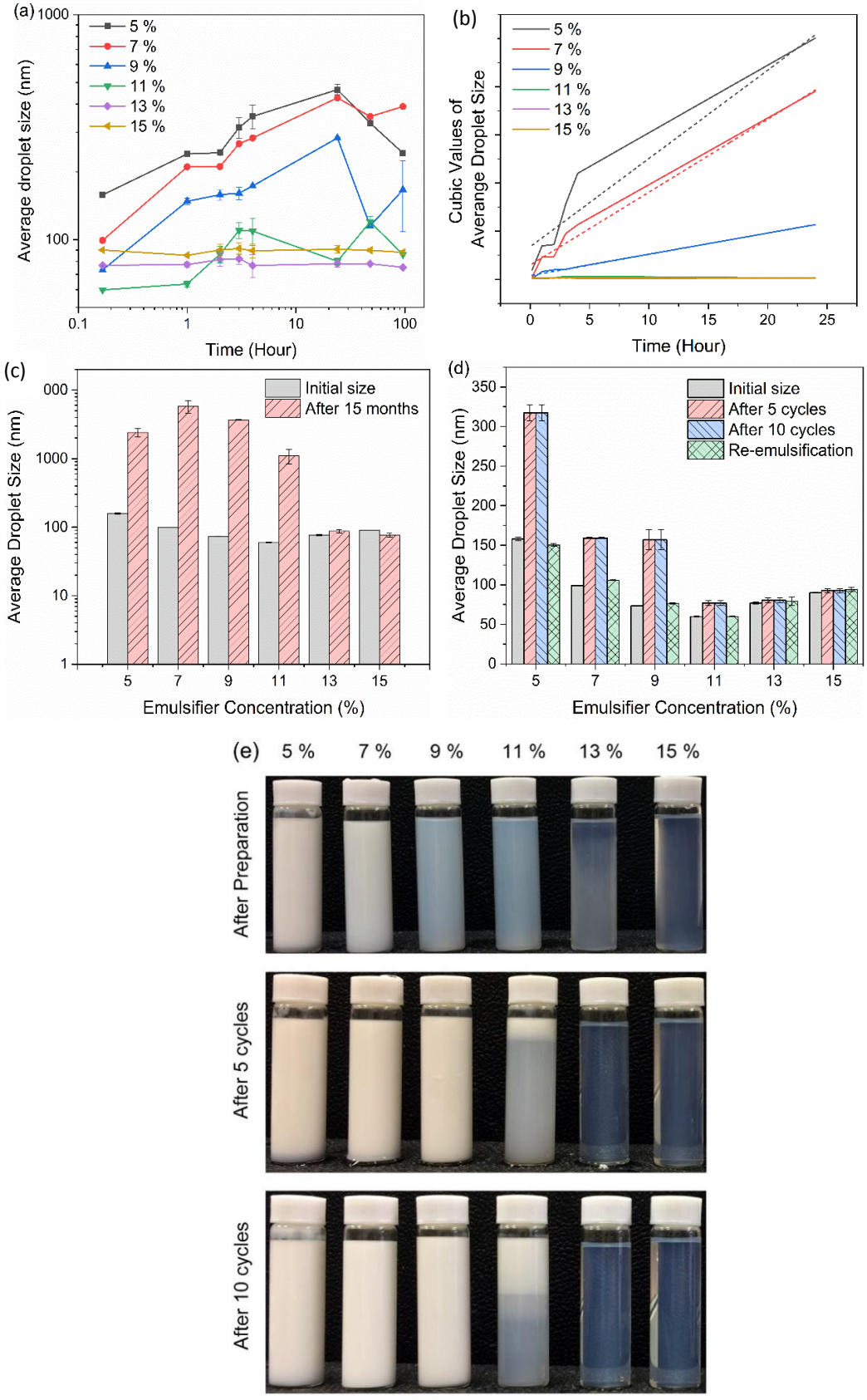


466 Fig. 8 Nano-emulsions prepared with different concentrations of Brij L4 and 30% PCM by the
467 PIT method: the changes in initial droplet sizes (a) and cubic values (b) over 25 h; (c) the initial

droplet sizes and after 15 months; (d) the initial droplet sizes and after freeze–thaw cycles, and re-emulsification; (e) the emulsion photos corresponding to c-d.

### 3.7. Overall discussion

The formation of nano-emulsions requires immense energy input than normal emulsions. The minimum energy required for generating droplets of a size of $a$, $\varepsilon_{min}$ is proportional to $3\gamma\phi_d^3/a$ ($\gamma$ = interfacial tension; $\phi_d$ = volume fraction of the dispersed phase) [43]. According to this relationship, the required energy input is lower when the interfacial tension is decreased. Therefore, in low energy emulsification methods, the interfacial tension is reduced to promote the formation of fine droplets at the inversion point. However, the emulsions are very unstable at low interfacial tension as coalescence is very fast [13]. Rapid cooling or heating is required to produce kinetically stable and fine emulsions (O/W or W/O, respectively) [44]. If the cooling or heating process is slow, coalescence predominates and polydisperse coarse emulsions form. Furthermore, when the viscosity is high, the phase inversion process could not finish at the inversion point, resulting in a more polydisperse droplet distribution. This also contributes to the different droplet sizes with PIT or EIP methods. Generally, the phase inversion occurs at a higher temperature in PIT emulsification than that in EIP and the corresponding viscosity could be lower than that at room temperature when the emulsifier concentration is lower than the CMC. Therefore, smaller droplets formed with the PIT method in section 3.1. When the emulsifiers were abundant, the opposite result appeared in 3.3 because the viscosity increased with the temperature increasing below 50 °C, the lowest point of the nonionic surfactants [36]. Also, according to sections 3.1 to 3.3, the droplet size distribution was not very dependent on the amount of water, implying that the droplet size was determined by the oil-to-emulsifier ratio, similar to that reported by other researchers [9, 12]. The appearance was found most transparent at PCM to emulsifier mass ratio of 2:1, which can be taken as the optimized ratio.

Compared with the normal emulsions of large droplets, the kinetic stability of nano-emulsions can be significantly enhanced by the small droplet size. As the most common instability mechanism in the normal PCM emulsions, coalescence occurs when the emulsion droplets collide to form a slight flattening deformation of the interface between the drops [7, 19, 28]. However, the droplet deformation associated coalescence is not common in nano-emulsions since the Laplace pressure, $\Delta P=2\gamma/r$, resisting deformation is orders of magnitude larger for nano-droplets than for micron-scale droplets [8, 13]. Ostwald ripening is the primary instability

mechanism for nano-emulsions, in which the poor solubility of the dispersed phase in the continuous phase results in molecular transfer between droplets. In a polydisperse emulsion, there is a mismatch in energy between droplets of differing size due to differences in interfacial energy, resulting in a driving force that produces a net flux of dispersed phase into larger droplets at the expense of smaller ones [40, 45]. The rate of droplet growth due to Ostwald ripening follows the Lifshitz–Slyozov–Wagner (LSW) theory as represented by Equation 1 [42]. In this study, most of the emulsion samples showed an excellent stability in a short period after their preparation and only a few remained stable over a long storage period in months. The slow destabilization of samples was largely attributed to the Ostwald ripening. As the ripened droplets increased in number, they may proceed to coalescence, creaming and other instability processes. The PCM nano-emulsions suitable for applications should have a long stability and a moderate or high viscosity. In a word, small droplet size and suitable viscosity are essential for a stable emulsion [7].

Based on the experimental results from the present study, the viscosity of an emulsion sample was increased with the emulsifier, and PCM concentrations and the addition of solid particles and the electrolyte. Most of the PCM nano-emulsions exhibited nearly Newtonian rheology at low shear rates, which is favorable for thermal storage applications. When the emulsifier concentration exceeds its CMC value in the continuous phase, formation of surfactant micelles increases the viscosity and may also turn the emulsion to non-Newtonian.

In emulsions formed with relatively high concentrations of PCM, the nano-sized droplets usually cause a higher viscosity. Compared with normal emulsions, nano-emulsions have a larger number of droplets in a given volume and the total droplet surface area can be several orders of magnitude larger than that of normal emulsions. The large surface area with the small nanodroplets creates stronger effects of Brownian motion, surface charge, adsorption, and hydration, increasing the emulsion viscosity [46]. In the case of repulsively driven particles at relatively high volume fractions, further increase in the volume fraction can cause rheological transition to a dynamically arrested state known as a colloidal glass [47]. A suspension of uniform rigid spheres transforms to the glassy behavior at $\phi_{d,glass} \sim 0.56$. However, due to the interaction forces among droplets, continuous phase and other components (e.g. surfactant micelles), the effective droplet volume is larger than the actual droplet volume. Therefore,

nano-emulsions can exhibit glass transition at significantly lower volume fractions, let to the high viscosity in sections 3.2 and 3.3. Furthermore, the addition of salts reduces the electrostatic repulsion and enhances the aggregation of droplets dominated by van der Waals attractions. Nevertheless, the aggregation did not lead to increasing instability of the emulsions and instead, to forming a shear-thinking gel structure. The movements of molecules and ions were limited with a low conductivity out of the PIT point.

## 4. Conclusions

In this work, n-hexadecane in water nano-emulsions were prepared with two low-energy emulsification methods and a working temperature of ~16 °C. The optimal formula was attained with Brij L4 (11-15%) and 30 % mass fraction of PCM and 2:1 PCM to emulsifier mass ratio, retaining a desirable fluidity of the emulsion. Nano-emulsions with small and uniform droplets were obtained by both methods with sufficient amount of emulsifiers. The final droplet sizes depended on the energy input and the phase inversion process during emulsification and the phase inversion temperature decreased with an increase in the emulsifier or the content of ethylene oxide group. The PCM nano-emulsions behaved as Newtonian liquid with a good fluidity and a superior stability during the long-time storage and freezing-cycles. Use of suitable emulsifiers was effective to generate stabile nano-emulsion droplets. Sufficient viscosity was another essential factor for the nano-emulsion stability, which was attained with a high concentration of emulsifiers or PCM. However, a very high viscosity could result from the highly dispersed PCM content and salt addition. Ostwald ripening was the dominant mechanism for the initial instability of diluted samples, followed by creaming and coalescence. Latent heat depends on the PCM content in the nano-emulsions. A high supercooling degree was observed in PCM nano-emulsions and the addition of hydrophobic $SiO_2$ NPs as a nucleating agent only reduced the supercooling moderately. Further studies are recommended to optimize the emulsification factors comprehensively and to develop more effective means for reduction of supercooling.

## Acknowledgments

This work was supported financially by the Research Grant Council of the Hong Kong SAR Government through RGC General Research Fund (PolyU 152707/16E) and by the Hong Kong Polytechnic University.

## References


1. Zhang, H.L., et al., *Thermal energy storage: Recent developments and practical aspects.* Progress in Energy and Combustion Science, 2016. **53**: p. 1-40.
2. Kousksou, T., et al., *Energy storage: Applications and challenges.* Solar Energy Materials and Solar Cells, 2014. **120**: p. 59-80.
3. Kant, K., A. Shukla, and A. Sharma, *Advancement in phase change materials for thermal energy storage applications.* Solar Energy Materials and Solar Cells, 2017. **172**: p. 82-92.
4. Sari, A. and A. Karaipekli, *Thermal conductivity and latent heat thermal energy storage characteristics of paraffin/expanded graphite composite as phase change material.* Applied Thermal Engineering, 2007. **27**(8-9): p. 1271-1277.
5. Wang, F., et al., *A comprehensive review on phase change material emulsions: Fabrication, characteristics, and heat transfer performance.* Solar Energy Materials and Solar Cells, 2019. **191**: p. 218-234.
6. Wang, F., X. Fang, and Z. Zhang, *Preparation of phase change material emulsions with good stability and little supercooling by using a mixed polymeric emulsifier for thermal energy storage.* Solar Energy Materials and Solar Cells, 2018. **176**: p. 381-390.
7. Zhang, X., J. Niu, and J.-Y. Wu, *Development and characterization of novel and stable silicon nanoparticles-embedded PCM-in-water emulsions for thermal energy storage.* Applied Energy, 2019. **238**: p. 1407-1416.
8. Gupta, A., et al., *Nanoemulsions: formation, properties and applications.* Soft matter, 2016. **12**(11): p. 2826-2841.
9. Ostertag, F., J. Weiss, and D.J. McClements, *Low-energy formation of edible nanoemulsions: Factors influencing droplet size produced by emulsion phase inversion.* Journal of Colloid and Interface Science, 2012. **388**(1): p. 95-102.
10. Engels, T., T. Förster, and W. Von Rybinski, *The influence of coemulsifier type on the stability of oil-in-water emulsions.* Colloids and Surfaces A: Physicochemical and Engineering Aspects, 1995. **99**(2): p. 141-149.
11. Morales, D., et al., *A study of the relation between bicontinuous microemulsions and oil/water nano-emulsion formation.* Langmuir, 2003. **19**(18): p. 7196-7200.
12. Fernandez, P., et al., *Nano-emulsion formation by emulsion phase inversion.* Colloids and

Surfaces A: Physicochemical and Engineering Aspects, 2004. **251**(1-3): p. 53-58.

13. Binks, B.P., *Modern aspects of emulsion science*. 1998: Royal Society of Chemistry.
14. Salager, J., et al., *Principles of emulsion formulation engineering*, in *Adsorption and Aggregation of Surfactants in Solution, vol. 109*, K.L. Mittal and O. Shah Dinesh, Editors. 2003, Marcel Dekker. p. 501-524.
15. Liu, W., et al., *Formation and stability of paraffin oil-in-water nano-emulsions prepared by the emulsion inversion point method.* Journal of Colloid and Interface Science, 2006. **303**(2): p. 557-563.
16. Xin, X., et al., *Influence of CTAB and SDS on the properties of oil-in-water nano-emulsion with paraffin and span 20/Tween 20.* Colloids and Surfaces A: Physicochemical and Engineering Aspects, 2013. **418**: p. 60-67.
17. Schalbart, P., M. Kawaji, and K. Fumoto, *Formation of tetradecane nanoemulsion by low-energy emulsification methods.* International Journal of Refrigeration, 2010. **33**(8): p. 1612-1624.
18. Schalbart, P. and M. Kawaji, *Comparison of paraffin nanoemulsions prepared by low-energy emulsification method for latent heat storage.* International Journal of Thermal Sciences, 2013. **67**: p. 113-119.
19. Zhang, X., et al., *PCM in Water Emulsions: Supercooling Reduction Effects of Nano-Additives, Viscosity Effects of Surfactants and Stability.* Advanced Engineering Materials, 2015. **17**(2): p. 181-188.
20. Jadhav, A.J., et al., *Ultrasound assisted manufacturing of paraffin wax nanoemulsions: Process optimization.* Ultrasonics Sonochemistry, 2015. **23**: p. 201-207.
21. Kawanami, T., et al., *Thermophysical properties and thermal characteristics of phase change emulsion for thermal energy storage media.* Energy, 2016. **117**: p. 562-568.
22. Chen, J. and P. Zhang, *Preparation and characterization of nano-sized phase change emulsions as thermal energy storage and transport media.* Applied Energy, 2017. **190**: p. 868-879.
23. Zhang, G. and C. Zhao, *Synthesis and characterization of a narrow size distribution nano phase change material emulsion for thermal energy storage.* Solar Energy, 2017. **147**: p. 406-413.

24. Cabaleiro, D., et al., *Development of paraffinic phase change material nanoemulsions for thermal energy storage and transport in low–temperature applications.* Applied Thermal Engineering, 2019: p. 113868.
25. Oró, E., et al., *Review on phase change materials (PCMs) for cold thermal energy storage applications.* Applied Energy, 2012. **99**: p. 513-533.
26. Huang, L., et al., *Subcooling in PCM emulsions-Part 1: Experimental.* Thermochimica Acta, 2010. **509**(1-2): p. 93-99.
27. Günther, E., et al., *Subcooling in hexadecane emulsions.* International Journal of Refrigeration, 2010. **33**(8): p. 1605-1611.
28. Zhang, X., J.-y. Wu, and J. Niu, *PCM-in-water emulsion for solar thermal applications: The effects of emulsifiers and emulsification conditions on thermal performance, stability and rheology characteristics.* Solar Energy Materials and Solar Cells, 2016. **147**: p. 211-224.
29. Zhao, Q., et al., *Graphene oxide Pickering phase change material emulsions with high thermal conductivity and photo-thermal performance for thermal energy management.* Colloids and Surfaces A: Physicochemical and Engineering Aspects, 2019. **575**: p. 42-49.
30. Wang, Y., et al., *Supercooling suppression and thermal behavior improvement of erythritol as phase change material for thermal energy storage.* Solar Energy Materials and Solar Cells, 2017. **171**: p. 60-71.
31. Höhne, G.W.H., W.F. Hemminger, and H.J. Flammersheim, *Differential Scanning Calorimetry*. 2003, Berlin, Heidelberg: Springer Berlin Heidelberg.
32. Coupland, J.N., *Crystallization in emulsions.* Current Opinion in Colloid and Interface Science, 2002. **7**(5-6): p. 445-450.
33. Tadros, T., et al., *Formation and stability of nano-emulsions.* Advances in Colloid and Interface Science, 2004. **108-109**: p. 303-318.
34. Rosen, M.J. and J.T. Kunjappu, *Surfactants and Interfacial Phenomena*. 4th ed. 2012, Hoboken, NJ, USA: John Wiley & Sons, Inc.
35. Perazzo, A., V. Preziosi, and S. Guido, *Phase inversion emulsification: Current understanding and applications.* Advances in colloid and interface science, 2015. **222**: p. 581-599.

36. Crook, E., D. Fordyce, and G. Trebbi, *Molecular weight distribution of nonionic surfactants. I. Surface and interfacial tension of normal distribution and homogeneous p, t-octylphenoxyethoxyethanols (OPE'S).* The Journal of Physical Chemistry, 1963. **67**(10): p. 1987-1994.
37. Bibette, J., et al., *Structure of adhesive emulsions.* Langmuir, 1993. **9**(12): p. 3352-3356.
38. Günther, E., et al., *Subcooling in PCM emulsions – Part 2: Interpretation in terms of nucleation theory.* Thermochimica Acta, 2011. **522**(1-2): p. 199-204.
39. Tadros, T., *Application of rheology for assessment and prediction of the long-term physical stability of emulsions*. Vol. 108-109. 2004. 227-258.
40. Tadros, T., et al., *Formation and stability of nano-emulsions.* Adv Colloid Interface Sci, 2004. **108-109**: p. 303-18.
41. Anton, N. and T.F. Vandamme, *Nano-emulsions and micro-emulsions: Clarifications of the critical differences.* Pharmaceutical Research, 2011. **28**(5): p. 978-985.
42. McClements, D.J., *Food Emulsions: Principles, Practices, and Techniques, Third Edition*. 2015: CRC Press. 690-690.
43. Helgeson, M.E., *Colloidal behavior of nanoemulsions: Interactions, structure, and rheology.* Current opinion in colloid & interface science, 2016. **25**: p. 39-50.
44. Solans, C., et al., *Nano-emulsions: formation, properties, and applications*, in *Adsorption and Aggregation of Surfactants in Solution, vol. 109*, K.L. Mittal and O. Shah Dinesh, Editors. 2003, Marcel Dekker: New York. p. 525-554.
45. Taylor, P., *Ostwald ripening in emulsions: Estimation of solution thermodynamics of the disperse phase.* Advances in Colloid and Interface Science, 2003. **106**(1-3): p. 261-285.
46. Perrin, J., *Brownian movement and molecular reality*. 2013: Courier Corporation.
47. Hunter, G.L. and E.R. Weeks, *The physics of the colloidal glass transition.* Reports on progress in physics, 2012. **75**(6): p. 066501.